Intrinsic Viscosity of Flexible Polymers in Couette and Poiseuille Flows

J. H. van Vliet and G. ten Brinke*

Department of Polymer Chemistry, University of Groningen, Nijenborgh 16, 9747 AG Groningen, The Netherlands

Received December 17, 1991; Revised Manuscript Received March 24, 1992

ABSTRACT: The zero-shear-rate intrinsic viscosity of a flexible polymer confined in a slit in Couette and Poiseuille flow is investigated by Monte Carlo simulations of self-avoiding random walks on a simple cubic lattice and by analytical calculations in the free-draining limit. In the simulations an equilibrium ensemble of chains is generated and the intrinsic viscosities in Newtonian Couette and Poiseuille flows are calculated by Zimm's algorithm. The intrinsic viscosity is calculated with hydrodynamic interaction and for the free-draining limit. There is a striking difference between both flow types with respect to the influence of the slit width on the intrinsic viscosity. As shown before,[7] the intrinsic viscosity in a Couette flow drops sharply from its unconfined value for distances between the plates for which the coils are squeezed. For a Poiseuille flow, on the other hand, the intrinsic viscosity starts to decrease gradually already at much larger distances. This difference is due to the fact that, due to the confinement, the polymers have a tendency to concentrate near the center of the slit, where in a Poiseuille flow the shear rate is 0. This occurs long before the real squeezing starts. In the limit of large slit widths the values coincide. These results are in agreement with analytical free-draining results and with calculations based on the Hookean dumbbell model of Goh et al.[31,32]

Introduction

The behavior of polymer solutions in confined flows is of great importance in hydrodynamic chromatography,[1,2] enhanced oil recovery,[3], drag reduction,[4,5] and (bio)lubrication.[6] The influence of polymer solutes on the zero-shear-rate intrinsic viscosity in a bounded and unbounded simple laminar shear flow, Couette flow, was discussed before.[7] The dependence of the zero-shear-rate intrinsic viscosity on the distance between the two parallel walls, L, which confine the Couette flow was discussed. For distances smaller than the distance at which the coils are squeezed,[14] the zero-shear-rate intrinsic viscosity, $[\eta]_L$, decreases sharply.

Since in practical applications confined pressure-driven flows, Poiseuille flows, are at least as equally important as Couette flows and since both Couette and Poiseuille flows are used to obtain data on the intrinsic viscosity of polymer solutions, it is worthwhile to compare both flow types.

In the model of Chauveteau et al.[3,8] for Poiseuille flow in a tube, the zero-shear-rate intrinsic viscosity as determined in unconfined flow, $[\eta]_0$, is used as an input parameter: the intrinsic viscosity is kept constant for all distances of the polymer chains to the pore wall and for all diameters of the pore concerned. Our previous results[7] on bounded Newtonian shear flow, however, show that the intrinsic viscosity depends on pore diameter, distance of polymer coils from the wall, and flow type.

The effects of confinement are noteworthy, i.e., the tendency of the polymer to avoid small pores,[9-11] the relative increase of the polymer segment density in the center of a single pore,[12,13] and the orientation and squeezing of the polymer coil in a pore.[14] These phenomena lead to viscosities different from a system in free space, i.e., where the distance between confining boundaries is much larger than the radius of gyration of a polymer coil.[3]

In this paper, Newtonian Couette and Poiseuille flows between two parallel walls are discussed. The flows are unidirectional and parallel to the walls with shear stress and shear rate constant in time. In Poiseuille flow the shear stress, and hence the shear rate, is not spatially invariant as for Couette flow but depends linearly on the coordinate perpendicular to the direction of flow.

The boundary walls are perpendicular to the z-direction and parallel to the direction of shear, x. The diameter of the slit is L, with $z = 0$ in the symmetry plane of the slit; i.e., $-L/2 \le z \le L/2$. The relation between shear stress, σ, shear rate, $\dot{\gamma}$, and viscosity, η, in these laminar flows is

$$\sigma = \eta\dot{\gamma} \quad \text{with } \dot{\gamma} = \mathrm{d}v_x/\mathrm{d}z, \quad v_y = v_z = 0 \tag{1}$$

where v_α is the α component of the velocity field, and $\alpha = x$, y, or z. For Couette flow σ and $\dot{\gamma}$ are independent of z. For Poiseuille flow σ and $\dot{\gamma}$ are[15]

$$\sigma = \frac{\partial \mathcal{P}}{\partial x} z \qquad \dot{\gamma} = \frac{\partial \mathcal{P}}{\partial x}\frac{1}{\eta} z \tag{2}$$

where $\mathcal{P}$ is the dynamic pressure.

In an unbounded flow σ and $\dot{\gamma}$ are as stated in eqs 1 and 2, but due to the finite distance between the plates, the values of σ and $\dot{\gamma}$ are changed near the boundary plates. In this paper we assume that the influence of the walls on σ and $\dot{\gamma}$ can be neglected. Such an assumption seems perfectly appropriate for simulations where the solvent is treated as a hydrodynamic continuum and the segments are implicitly assumed to be entities much larger than the solvent molecules. Friction with the repulsive walls is assumed to be absent. Experimentally, these assumptions will break down when the distance between the walls is too small to ignore slip of the solvent or the molecular nature of polymer chain, wall, and solvent.[16-19] If the shear stress is not a constant, as in Poiseuille flow, the polymer chains prefer regions with the lowest shear stress.[20-23] Since we are interested in the limit $\dot{\gamma} \to 0$ and $\sigma \to 0$, it seems reasonable enough to neglect this effect on the polymer conformations.

Results are obtained with hydrodynamic interaction (HI) between chain segments and between segments and the boundary walls. To assess the effect of HI, and as a check on the numerical algorithms used, the free-draining limit (FD) is considered as well.

0024-9297/92/2225-3695$03.00/0

The basics of the model to calculate $[\eta]_L$ can be found in the literature.[7,24] Essential is the use of the spatial distribution function of the polymer chain at rest,[25] the treatment of a polymer conformation as a rigid body,[26] and the use of a modified Oseen tensor to model HI.[28,29]

In Couette flow the contribution to the zero-shear-rate intrinsic viscosity from a single polymer conformation is[26,27]

$$[\eta]_L = -\frac{N_A}{M}\frac{1}{\eta_0}(1/\dot\gamma)\sum_i^{N+1} z_i F_{i,x} \tag{3}$$

where N_A is Avogadro's number, M is the molecular weight, η_0 is the solvent viscosity, and $\mathbf{F}_i$ is the friction force on the ith chain segment. The only forces acting on the chain segments in this model are the friction forces. In the steady state, the net force acting on the center of mass, averaged over all conformations, is zero[2]

$$\sum_i^{N+1} \langle F_{i,x}\rangle = 0 \tag{4}$$

Equations 3 and 4 give for the intrinsic viscosity

$$\langle[\eta]_L\rangle = -\frac{N_A}{M}\frac{1}{\eta_0}(1/\dot\gamma)\sum_i^{N+1}\langle z_i' F_{i,x}\rangle \qquad z_i' = z_i - z_{CM} \tag{5}$$

The superscript prime indicates a coordinate relative to the coil's center of mass. The superscript CM indicates the center of mass.

The equation for the zero-shear-rate intrinsic viscosity in Poiseuille flow may be obtained from a consideration of energy dissipation in a way quite similar to a well-known procedure for Couette flow, leading to eq 3.[26,27]

If $\mathbf{v}_i^0$ is the original velocity of the solvent fluid at the point of location of the ith segment, the work done in unit time by the fluid for the ith segment is $-\mathbf{F}_i\mathbf{v}_i^0$. The Poiseuille flow is a laminar flow in the x direction with $v_{i,x}^0 = -(\partial\mathcal{P}/\partial x)(1/\eta)(1/2)[(L/2)^2 - z_i^2]$. The increase in energy loss in unit time and in unit volume due to the presence of ρ polymer chains per unit volume is therefore (using eqs 2 and 4) equal to

$$W_P = -\rho/2\sum_i^{N+1}\dot\gamma(z_i)\, z_i F_{i,x} \tag{6}$$

Now the slit is divided in infinitesimal slices of width dz, in which the shear rate $\dot\gamma(z) = Gz$, with $G = (\partial\mathcal{P}/\partial x)\cdot(1/\eta)$ constant. In the infinitesimal slice, the energy dissipation may be obtained by considering a Couette flow between two parallel plates at a distance dz.[27] Suppose that one of the two parallel plates of area A at a distance dz is moving with a velocity $d\upsilon = \dot\gamma(z)\, dz$ with respect to the other. Then the frictional force on the moving plate is $F = \eta\dot\gamma(z)\, A$, and the displacement of this plate per unit time is $d\upsilon = \gamma(z)\, dz$. Furthermore, the total amount of work dissipated in the volume $A\, dz$ per unit time is

$$F\, d\upsilon = \eta\dot\gamma(z)^2\, A\, dz \tag{7}$$

By integration of eq 7 over the slit width the energy dissipation per unit time in the Poiseuille flow is obtained as

$$(AL)W = \int_{-L/2}^{L/2}\eta G^2 z^2 A\, dz = (AL)\eta\frac{L^2}{12}G^2 \tag{8}$$

Writing the energy dissipation per unit volume and unit time, W, as $W = W_0 + W_p$, with W_0 the solvent contribution to W, gives

$$W_p = (\eta - \eta_0)\frac{L^2}{12}G^2 \tag{9}$$

Combining eqs 6 and 9 gives for the zero-shear-rate intrinsic viscosity in Poiseuille flow

$$[\eta]_L = -\frac{N_A}{M}\frac{1}{\eta_0}\frac{6}{L^2G}\sum_i^{N+1} z_i^2 F_{i,x} \tag{10}$$

With eq 4 $[\eta]_L$ is written as

$$[\eta]_L = -\frac{N_A}{M}\frac{1}{\eta_0}\frac{6}{L^2G}\sum_i^{N+1}(z_i'^2 + 2z_{CM}z_i')F_{i,x} \tag{11}$$

Conformational averages of $[\eta]_L$ obtained analytically for Poiseuille flow will be calculated further on with the equation

$$\langle[\eta]_L\rangle = (1/L)\int_{-L/2}^{L/2}\langle[\eta]_L\rangle_{CM}\, dz_{CM} \tag{12}$$

where the angular brackets indicate an average over polymer conformations and the angular brackets with index CM a conformational average with z_{CM} fixed.

The above discussion on energy dissipation in a Poiseuille flow (eqs 11 and 12) is valid if the correlation length along the chain, b (Kuhn's segment length), is such that the change of $\dot\gamma(z)$ over a distance $b\,|\cos\theta|$ is small

$$\frac{\partial\mathcal{P}}{\partial x}\frac{1}{\eta}b|\cos\theta| \to 0 \tag{13}$$

or since $|\cos\theta|_{MAX} = 1$, $(\partial\mathcal{P}/\partial x)(1/\eta)b \to 0$, where θ is the angle between the z-axis and Kuhn's segment. In our model of a flexible polymer we are interested in the limit $\dot\gamma \to 0$, so $(\partial\mathcal{P}/\partial x)(1/\eta) \to 0$ and eq 13 is satisfied automatically.

For confined systems averages over polymer conformations depend on L. Hence, the angular velocity is a function of L. In Zimm's procedure the angular velocity Ω_L of a polymer conformation is defined as[2,26,30]

$$\Omega_L \equiv C\frac{\langle\sum_i^{N+1} z_i'^2\rangle}{\langle\sum_i^{N+1}(x_i'^2 + z_i'^2)\rangle} \qquad \Omega_\infty = C/2 \tag{14}$$

The above defining eq 14 requires a priori knowledge of $\langle\sum_i^{N+1} z_i'^2\rangle$ and $\langle\sum_i^{N+1} x_i'^2\rangle$ to calculate $[\eta]_L$. To avoid this, we set the angular velocity for all distances L equal to Ω_∞ or define an angular velocity ω_L for an individual conformation. The definition of ω_L is

$$\omega_L \equiv C\frac{\sum_i^{N+1} z_i'^2}{\sum_i^{N+1}(x_i'^2 + z_i'^2)} \tag{15}$$

In the following, both cases of a conformational-independent angular velocity $\omega = \Omega_\infty$ and a conformational-dependent angular velocity $\omega = \omega_L$ will be considered and the consequences discussed. The expressions for Ω_L and ω_L in Poiseuille and Couette flow differ in the value of C only (Table I).[2]

An explicit comparison between our model for Couette and Poiseuille flow with the model of Goh et al.[31,32] for a dilute dumbbell suspension is made. The dumbbell

Table I
Type of Flow

	Couette flow	Poiseuille flow
C	$\dot{\gamma}$	$\dot{\gamma}_{CM} = \frac{\partial \mathcal{P}}{\partial x}\frac{1}{\eta} z_{CM}$
$u_{CM,x}$	$\dot{\gamma} z_{CM}$	$-\frac{\partial \mathcal{P}}{\partial x}\frac{1}{2\eta}[(L/2)^2 - z_{CM}^2 - \{\sum_i^{N+1} z_i'^2/(N+1)\}]$
$v_{i,x}^{r,t}$	$-\dot{\gamma} z_i'$	$-\frac{\partial \mathcal{P}}{\partial x}\frac{1}{2\eta}[2z_{CM}z_i' + z_i'^2 - \{\sum_i^{N+1} z_i'^2/(N+1)\}]$

consists of two beads of negligible mass connected by a linear Hookean spring.[33] The probability density function of the dumbbell conformation is assumed independent of the dumbbell's center of mass. The bead radius is assumed small compared to the end-to-end distance, R_0, of the dumbbell, so reflection occurs when a bead center attempts to cross the boundary walls. Interaction between dumbbells as well as HI is neglected. The equations derived by Goh et al. for the specific viscosity translated into our notation are eqs 16–19.

for Couette flow

$$\frac{\langle[\eta]_L\rangle}{\langle[\eta]_0\rangle} = 2[(2/\lambda)^{1/2}\int_0^{(2\lambda)^{1/2}}\mathrm{erf}\,(\vartheta)\,d\vartheta]^{-1} \times \frac{1}{(2\lambda)^{1/2}}\int_0^{(2\lambda)^{1/2}}\left(\mathrm{erf}\,(\xi) - \frac{2}{(2\pi)^{1/2}}\xi e^{-\xi^2}\right)d\xi \quad (16)$$

for Poiseuille flow

$$\frac{\langle[\eta]_L\rangle}{\langle[\eta]_0\rangle} = 4[(2/\lambda)^{1/2}\int_0^{(2\lambda)^{1/2}}\mathrm{erf}\,(\vartheta)\,d\vartheta]^{-1} \times \frac{1}{(2\lambda)^{1/2}}\left[\int_0^{(2\lambda)^{1/2}}\left(\mathrm{erf}\,(\xi) - \frac{2}{(2\pi)^{1/2}}\xi e^{-\xi^2}\right)d\xi - \frac{1}{(2\lambda)^{1/2}}\int_0^{(2\lambda)^{1/2}}\xi\left(\mathrm{erf}\,(\xi) - \frac{2}{(2\pi)^{1/2}}\xi e^{-\xi^2}\right)d\xi\right] \quad (17)$$

where erf ( ) denotes the error function and $\lambda = (3/4)(L/R_0)^2$. In the limit of $R_0/L \to 0$ the asymptotic solution of eq 16 is

$$\frac{\langle[\eta]_L\rangle}{\langle[\eta]_0\rangle} = \left[1 - \frac{2}{(6\pi)^{1/2}}\frac{R_0}{L}\right] \quad (18)$$

and of eq 17 is

$$\frac{\langle[\eta]_L\rangle}{\langle[\eta]_0\rangle} = \left[1 - \frac{4}{(6\pi)^{1/2}}\frac{R_0}{L} + \left(\frac{R_0}{L}\right)^2\right] \quad (19)$$

with values of $\langle[\eta]_0\rangle$ equal in Couette and Poiseuille flow. For this Hookean dumbbell the intrinsic viscosity is independent of shear rate and does not show shear thinning. Its applicability is limited to the low-shear-rate regime. To compare our results with the dumbbell results, R_0 is identified with either the end-to-end distance or with twice the length of the largest principal axis of the ellipsoid defined by the radius of gyration tensor of a self-avoiding random walk (SAW). The orientation of the axis is defined by the eigenvector for this eigenvalue. Although both choices for R_0 are somewhat arbitrary, the latter identification for R_0 is motivated by the fact that the largest principal axis seems to be the characteristic length relevant to the confinement of polymer chains in a slit.[14]

Model and Simulation Method

Monte Carlo simulations of an athermal SAW on a simple cubic lattice with periodic boundary conditions in the x- and y-direction were performed. The two parallel walls were perpendicular to the z-axis. The length of the lattice in the directions with periodic boundary conditions varied with the chain length considered. In all these cases, this length exceeded the root-mean-square end-to-end distance of the SAW. The number of steps of the SAW's were $N = 59, 79$, and 150. For each chain length considered, the lattice length in the x- and y-direction was fixed. For the shortest distance between the walls considered, the densities, expressed as the fraction of lattice sites occupied, varied between 0.8% for $N = 59$ and 0.9% for $N = 150$. With larger distances between the walls, the densities were correspondingly lower. The largest distance between walls was $L = 121$. For each chain length and distance between the walls, a representative sample was obtained by the reptation algorithm. To speed up equilibration, chain growth and reptation took place simultaneously.

The first 2×10^6 attempted moves after completion of chain growth were ignored. From the subsequent interval of 2×10^6 attempted moves 26 times, at equally spaced intervals, quantities of interest were calculated and averaged afterward. This procedure was repeated for five independent runs. After averaging again, the statistical errors were calculated as usual from the averages per run.

In Zimm's procedure[26] for the calculation of the zero-shear-rate intrinsic viscosity, the polymer coil is considered to be a rigid body. In our adaptation to the confined situation it is assumed that the coil does not rotate if it is hindered by either of the walls, which is the case if the following two conditions are satisfied. The first condition is that one or more segments of the SAW are in a lattice layer one step length apart from either of the boundary walls. For Couette flow the second condition is that for at least one of these segments the coordinate in the direction of shear relative to the coil's center of mass is positive in one layer or negative in the other. Due to symmetry it is irrelevant which layer is associated with which sign of the segment coordinate, but the coupling should be fixed during one computer run. For Poiseuille flow the angular velocity changes sign when the center of mass of the coil passes through the center of plane at $z = 0$. In the case of Poiseuille flow, therefore, the second condition is modified; the association of a positive or negative segment with each of the boundary layers is reversed when the center of mass passes through the center plane. If rotation is hindered, we assume for the angular velocity $\omega = 0$ as before.[7] Then each segment of the coil has a translational velocity component equal to the velocity of the center of mass. The basic equations can be found elsewhere;[26,27] however, to clarify the above considerations, we will give a brief overview of the equations involved

$$\mathbf{v}_i = \mathbf{v}_i^0 + \mathbf{v}_i^* \quad (20)$$

$$\mathbf{F}_i = \zeta(\mathbf{u}_i - \mathbf{v}_i) \qquad \zeta = 6\pi\eta_0 a \qquad \eta_0 = 1 \quad (21)$$

$$\mathbf{v}_i^* = \sum_{i \neq j}^{N+1} \mathbf{T}_{ij}\mathbf{F}_j \quad (22)$$

where $\mathbf{v}_i^0$ is the velocity of the solvent at the position of the ith segment if that segment would have been absent, $\mathbf{u}_i$ is the velocity of the ith segment, ζ is the friction coefficient of a segment, a is the Stokes radius of a segment in step length units ($a = 1/2$), $\mathbf{F}_i$ is the friction force exerted

on the solvent by a segment, $\mathbf{v}_i^*$ is the contribution to $\mathbf{v}_i$ due to hydrodynamic perturbation from all other segments of the polymer chain, and $\mathbf{T}$ is the Oseen tensor. Equations 20–22 give the equations to be solved numerically,[26] with HI

$$(1/\zeta)\mathbf{F}_i + \sum_{i \neq j}^{N+1} \mathbf{T}_{ij}\mathbf{F}_j = \mathbf{u}_i - \mathbf{v}_i^0 \tag{23}$$

or in the case of FD

$$(1/\zeta)\mathbf{F}_i = \mathbf{u}_i - \mathbf{v}_i^0 \tag{24}$$

Both Couette and Poiseuille flows are laminar with

$$\mathbf{v}_i^0 = \begin{pmatrix} v_{i,x}^0(z) \\ 0 \\ 0 \end{pmatrix} \tag{25}$$

As the chain is assumed to behave as a rigid body, the velocity of the ith segment is

$$\mathbf{u}_i = \mathbf{u}_{CM} + \omega \times \mathbf{R}_i \tag{26}$$

$$\omega = \begin{pmatrix} 0 \\ \omega \\ 0 \end{pmatrix} \qquad \mathbf{u}_{CM} = \begin{pmatrix} u_{CM,x} \\ 0 \\ 0 \end{pmatrix}$$

where $\mathbf{R}_i$ is the position vector of the ith segment with respect to the center of mass, $\mathbf{u}_{CM}$ is the velocity of the center of mass, and ω is the angular velocity vector of the polymer chain. The choice made for ω is $\omega = \omega_L$ or $\omega = \Omega_\infty$. The velocity $\mathbf{v}_i^r = \mathbf{u}_i - \mathbf{v}_i^0$ can be written as

$$\mathbf{v}_i^r = \mathbf{v}_i^{r,t} + \mathbf{v}_i^{r,r} \qquad \mathbf{v}_i^{r,t} = \mathbf{u}_{CM} - \mathbf{v}_i^0 \qquad \mathbf{v}_i^{r,r} = \omega \times \mathbf{R}_i \tag{27}$$

$$\mathbf{v}_i^{r,t} = \begin{pmatrix} v_{i,x}^{r,t} \\ 0 \\ 0 \end{pmatrix}, \quad \text{and} \quad \mathbf{v}_i^{r,r} = \begin{pmatrix} \omega z_i' \\ 0 \\ -\omega x_i' \end{pmatrix} \tag{28}$$

If rotation is impossible ($\omega = 0$)

$$\mathbf{v}_i^r = \mathbf{v}_i^{r,t} \qquad \mathbf{v}_i^{r,t} = \mathbf{u}_{CM} - \mathbf{v}_i^0 \qquad \mathbf{v}_i^{r,r} = 0 \tag{29}$$

The dimensionless quantity actually computed is $E_L \sim [\eta]_L$.[26] For Couette flow

$$E_L = (-2/\dot{\gamma})\sum_i^{N+1} z_i' F_{i,x} \tag{30}$$

and for Poiseuille flow

$$E_L = -\frac{12}{L^2 G}\sum_i^{N+1} (z_i'^2 + 2\, z_{CM} z_i') F_{i,x} \tag{31}$$

In the steady state the average moment of the force about the center of mass is zero:[2] $\sum_i^{N+1} z_i' F_{i,x} = \sum_i^{N+1} x_i' F_{i,z}$. This can be used to reduce the statistical errors in E_L if calculated by a Monte Carlo method: for a single conformation both $z_i' F_{i,x}$ and $x_i' F_{i,z}$ terms can be used in the computation of E_L.[26] The substitutions of quantities necessary in eq 28 for Couette and Poiseuille flow are given in Table I and eqs 14 and 15.

The HI of a segment with each of the walls is modeled as the HI of a solid sphere with a wall. As $a = 1/2$ and the distance d_i between one of the walls and the ith segment in step length units satisfies $d_i \geq 1$, results on HI published for $a/d_i \ll 1$ are used. Corrections to the HI with both walls are superimposed, and only terms linear in a/d_i are retained for the diagonal elements of the Oseen tensor:[34,35]

no HI between segments and the walls

$$T_{ii}^{xx} = T_{ii}^{yy} = T_{ii}^{zz} = 1/\zeta \tag{32}$$

HI between segments and the walls

$$T_{ii}^{xx} = T_{ii}^{yy} = (1/\zeta)\left(1 - \frac{9}{16}\frac{aL}{(L-d_i)d_i} + \ldots\right) \tag{33}$$

$$T_{ii}^{zz} = (1/\zeta)\left(1 - \frac{9}{8}\frac{aL}{(L-d_i)d_i} + \ldots\right) \tag{34}$$

Results and Discussion

Characteristic lengths of athermal SAW's in three dimensions, like the radius of gyration and end-to-end distance, scale with N^ν. The Flory scaling exponent for an excluded-volume chain is $\nu = 0.6$.[36,37] The most accurate value available to date for a SAW on a simple cubic lattice is $\nu = 0.592$.[38,39] To compare results for different values of N, the distance between the walls is expressed in units Δ defined by

$$\Delta \equiv L/N^\nu \tag{35}$$

The following equations are all derived for the FD limit. These equations are presented to clarify some of the Monte Carlo results. From now on the superscript R indicates a rotating conformation ($\omega \neq 0$) and the superscript T indicates a sliding conformation ($\omega = 0$). Equations 36–41 are obtained with eqs 24, 27, and 28 and Table I, setting $\omega = \Omega_\infty$. For Couette flow, using eq 5, the conformational averages are

$$\langle [\eta]_L^R \rangle = \frac{N_A}{M}\frac{1}{\eta_0}\frac{1}{\zeta}\frac{1}{2}\sum_i^{N+1}\langle z_i'^2 \rangle \tag{36}$$

$$\langle [\eta]_L^T \rangle = \frac{N_A}{M}\frac{1}{\eta_0}\frac{1}{\zeta}\sum_i^{N+1}\langle z_i'^2 \rangle \tag{37}$$

For Poiseuille flow with the use of eq 11 and realizing that odd powers of z_i' disappear, conformational averages (for z_{CM} fixed) are

$$\langle [\eta]_L^R \rangle_{CM} = \frac{N_A}{M}\frac{1}{\eta_0}\frac{6}{L^2}\frac{1}{\zeta}\sum_i^{N+1}(z_{CM}^2\langle z_i'^2 \rangle_{CM} + \langle z_i'^4 \rangle_{CM} - \langle z_i'^2 \sum_k^{N+1} z_k'^2/(N+1)\rangle_{CM}) \tag{38}$$

$$\langle [\eta]_L^T \rangle_{CM} = \frac{N_A}{M}\frac{1}{\eta_0}\frac{6}{L^2}\frac{1}{\zeta}\sum_i^{N+1}(2z_{CM}^2\langle z_i'^2 \rangle_{CM} + \langle z_i'^4 \rangle_{CM} - \langle z_i'^2 \sum_k^{N+1} z_k'^2/(N+1)\rangle_{CM}) \tag{39}$$

Decoupling the position of the center of mass from the averages for a fixed coordinate z_{CM} is valid in the limit $\Delta \to \infty$. Using eq 12 gives the conformational averages

$$\langle [\eta]_L^{R} \rangle = \frac{N_A}{M}\frac{6}{\eta_0}\zeta\sum_i^{N+1}\left(\frac{\langle z_i'^2\rangle}{12} + \frac{\langle z_i'^4\rangle}{L^2} - \frac{\langle z_i'^2\sum_k^{N+1} z_k'^2/(N+1)\rangle}{L^2}\right) \quad (40)$$

$$\langle [\eta]_L^{T} \rangle = \frac{N_A}{M}\frac{6}{\eta_0}\zeta\sum_i^{N+1}\left(\frac{\langle z_i'^2\rangle}{6} + \frac{\langle z_i'^4\rangle}{L^2} - \frac{\langle z_i'^2\sum_k^{N+1} z_k'^2/(N+1)\rangle}{L^2}\right) \quad (41)$$

In the limit $L \to \infty$ eqs 40 and 41 reproduce eqs 36 and 37 for Couette flow.

In Table II results are presented for $\Delta > 6$. Simulation data on the intrinsic viscosity in unbounded Couette flow were published in a previous paper.[7] The data are also reported in Table II. The values of the intrinsic viscosity in FD can be calculated analytically for unbounded Couette flow with eqs 30 and 36. These values are also tabulated. It is clear now that for $\Delta > 6$ Couette flow is essentially unconfined: for FD the analytical values of E_L in Couette flow are in excellent agreement with the numerical simulation results. It is obvious that in the large slit-width limit, the results for Couette and Poiseuille flow coincide for HI as well as in the FD limit. For FD this is shown by the eqs 36, 37, 40, and 41.

For Couette flow eqs 5, 14, 15, 24, 27, and 28 and Table I give in the FD limit

$$\langle [\eta]_L^{R} \rangle_{\omega_L} = \frac{N_A}{M}\frac{1}{\eta_0}\zeta\left\langle\left(\frac{1}{A} + \frac{1}{B}\right)^{-1}\right\rangle \quad (42)$$

$$\langle [\eta]_L^{R} \rangle_{\Omega_L} = \frac{N_A}{M}\frac{1}{\eta_0}\zeta\left(\frac{1}{\langle A\rangle} + \frac{1}{\langle B\rangle}\right)^{-1} \quad (43)$$

where $A \equiv \sum_i^{N+1} z_i'^2$ and $B \equiv \sum_i^{N+1} x_i'^2$. Equations 42 and 43 and some simple statistics prove

$$\delta \equiv \langle [\eta]_L^{R} \rangle_{\omega_L} - \langle [\eta]_L^{R} \rangle_{\Omega_L} < 0 \quad (44)$$

in agreement with the data in Table II. In the limit $\Delta \to \infty$ the scaling behavior of δ is that of $[\eta]_0$ in FD[30]

$$\delta \sim N^{2\nu} \quad (45)$$

Assuming the same functional relation between δ and $[\eta]_0$ in the nondraining limit (infinite HI) gives[40]

$$\delta \sim N^{3\nu-1} \quad (46)$$

Not enough different chain lengths have been investigated to test these scaling predictions quantitatively. Qualitatively, the correct behavior is observed.

Figures 1–5 show $E_L/E_0 = [\eta]_L/[\eta]_0$ as a function of Δ for various different situations. The value of E_0 is the value of E_L for Couette and Poiseuille flow with $L = 121$ as given in Table II. Results for FD as well as results for HI are presented. The values of E_L/E_0 with $N = 59$ are somewhat higher than with $N = 79$ and $N = 150$ especially with $\omega = \omega_L$. It indicates that $N = 59$ with $\omega = \omega_L$ is not in the long chain limit for E_L/E_0.[7,14] From Figures 1–4 it is obvious that in Poiseuille flow E_L/E_0 is less than E_L/E_0 in Couette flow. E_L/E_0 for Couette flow decreases for $\Delta \leq 1.5$, when the coil is squeezed.[14] For larger values of Δ, $E_L/E_0 = 1$. For Poiseuille flow it is obvious that E_L/E_0 increases continuously with increasing Δ. In the limit of large slit widths also for Poiseuille flow $E_L/E_0 \to 1$. This was already discussed above for FD (Table II). This difference in behavior is due to the tendency of the polymer coils to concentrate near the center of the slit. This tendency, which is already present at distances between the plates that are much larger than the distance at which the squeezing starts, reduces the viscosity in a Poiseuille flow because of the parabolic velocity profile with a shear rate 0 in the center of the plates.

Comparison of Figure 1 with Figure 2, and Figure 3 with Figure 4, shows that the data scatter in E_L/E_0 for $\omega = \omega_L$ is larger than that for $\omega = \Omega_\infty$. This is due to the fact that Ω_∞ is fixed for all L, while ω_L on the other hand is a conformational property prone to statistical fluctuations (eqs 14 and 15). Values of E_L/E_0 are slightly larger with $\omega = \omega_L$ than with $\omega = \Omega_\infty$. This is due to the fact that, for $\Delta \to 0$, ω_L goes to zero, while Ω_∞ is constant for all Δ. With

Table II
E_L for $\Delta > 6$ and $\Delta \to \infty$[a]

			E_L^{HI}		E_L^{FD}		
N	L	flow type	Ω_∞	ω_L	Ω_∞	ω_L	E_∞^{FD}: Ω_∞
59	∞	Couette	22		71		
	121	Couette	21	16	66	46	70
	121	Poiseuille	17	12	54	36	
79	∞	Couette	27		101		
	121	Couette	28	23	104	81	98
	121	Poiseuille	27	24	100	87	
150	∞	Couette	40		201		
	121	Couette	43	35	221	170	210
	121	Poiseuille	34	28	173	135	

[a] E_∞^{FD} is E_L^{FD} calculated from $\langle [\eta]_L^{R} \rangle$ for $\Delta \to \infty$ with eqs 30 and 36. $E_\infty^{FD} = 0.1772\pi N^{1.184}$ (see also ref 38).

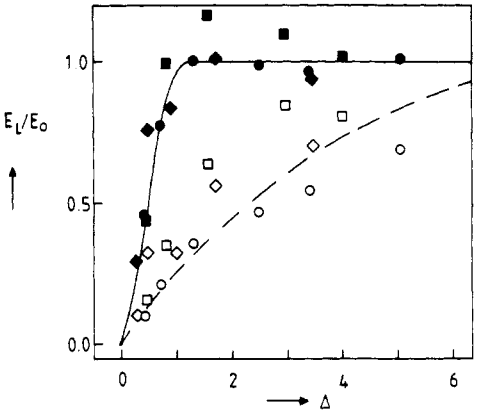

Figure 1. E_L/E_0 as a function of Δ, with $\omega = \omega_L$ and HI: (■,□) $N = 59$; (●,○) $N = 79$; (◆,◇) $N = 150$. Open symbols and dashed line: Poiseuille flow. Solid symbols and solid line: Couette flow. Maximum error is 0.28 in Couette and 0.18 in Poiseuille flow.

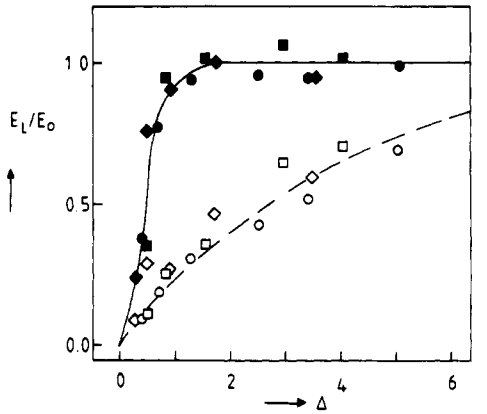

Figure 2. E_L/E_0 as a function of Δ, with $\omega = \Omega_\infty$ and HI: (■,□) $N = 59$; (●,○) $N = 79$; (◆,◇) $N = 150$. Open symbols and dashed line: Poiseuille flow. Solid symbols and solid line: Couette flow. Maximum error is 0.26 in Couette and 0.15 in Poiseuille flow.

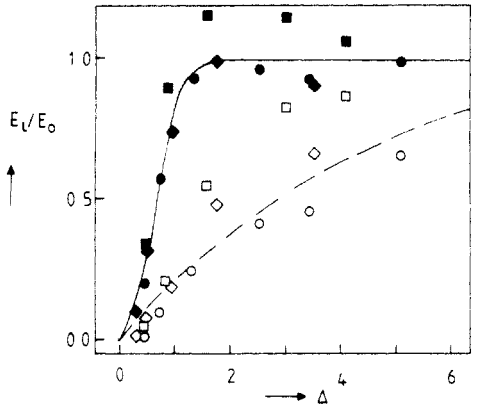

Figure 3. E_L/E_0 as a function of Δ, with $\omega = \omega_L$ and FD: (■,□) $N = 59$; (●,○) $N = 79$; (◆,◇) $N = 150$. Open symbols and dashed line: Poiseuille flow. Solid symbols and solid line: Couette flow. Maximum error is 0.13 in Couette and 0.16 in Poiseuille flow.

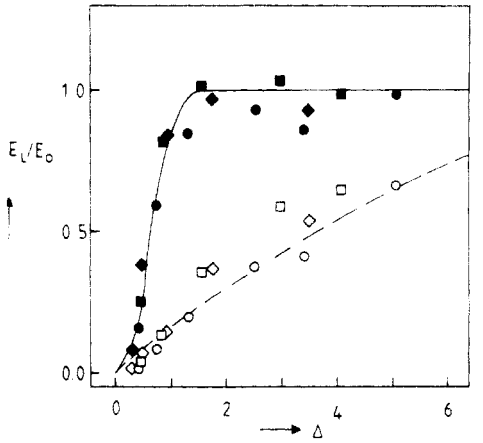

Figure 4. E_L/E_0 as a function of Δ, with $\omega = \Omega_\infty$ and FD: (■,□) $N = 59$; (●,○) $N = 79$; (◆,◇) $N = 150$. Open symbols and dashed line: Poiseuille flow. Solid symbols and solid line: Couette flow. Maximum error is 0.09 in Couette and 0.11 in Poiseuille flow.

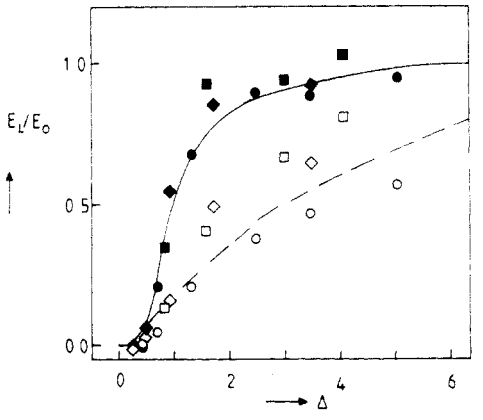

Figure 5. Contribution of conformations *not* hindered by the walls, to E_L/E_0 as a function of Δ, with $\omega = \omega_L$ and HI: (■,□) $N = 59$; (●,○) $N = 79$; (◆,◇) $N = 150$. Open symbols and dashed line: Poiseuille flow. Solid symbols and solid line: Couette flow. Maximum error is 0.50 in Couette and 0.42 in Poiseuille flow.

$\omega = 0$ the coils slide, this gives a higher intrinsic viscosity than with $\omega \neq 0$ for both flow types (eqs 36, 37, and 38, 39).

From Figure 5 it is obvious that in Couette and Poiseuille flow the major part of the intrinsic viscosity is contributed by conformations which do not touch either of the walls. Table III shows that there is no significant difference between results for the contribution of conformations not hindered by the walls to E_L, considering either $\omega = \omega_L$ or $\omega = \Omega_\infty$ for Poiseuille flow. Only when the slit width is large compared to the coil's size ($L = 121$) is there a significant difference for Poiseuille flow. For Couette flow, on the other hand, this contribution to E_L is larger with Ω_∞ than with ω_L as expected from eqs 44–46. These differences are explained by the fact that for Couette flow all conformations not hindered by either of the walls do rotate; for Poiseuille flow, on the other hand, conformations with their center of mass in the middle plane of the slit also slide, just as the conformations hindered by the walls.

Table III
Contribution of Nonhindered Conformations to E_L with $N = 150$

		E_L^{HI}		E_L^{FD}	
L	flow type	Ω^∞	ω_L	Ω_∞	ω_L
5	Couette	0	0	0	0
	Poiseuille	0	0	0	0
9	Couette	8	2.6	38	8.4
	Poiseuille	0.6	0.6	1.0	1.1
17	Couette	29	19	136	77
	Poiseuille	4.7	4.7	12	13
33	Couette	38	30	186	140
	Poiseuille	14	14	53	54
67	Couette	41	33	204	154
	Poiseuille	19	19	84	81
121	Couette	42	34	216	164
	Poiseuille	33	27	165	128

The effect of HI is a very slight increase of E_L/E_0, compared to the FD limit for both $\omega = \omega_L$ (Figures 1 and 3) and $\omega = \Omega_\infty$ (Figures 2 and 4). A priori one would expect an increase of the intrinsic viscosity as the effective friction with the wall is enhanced (eqs 32–34). That the effect is only marginal is basically due to the tendency of the polymer segments to concentrate in the center of the slit, away from the walls. In the region where the coil is squeezed with $\Delta \leq 1.5$,[14] an additional effect might come into play, reducing the importance of HI, as indicated by some theoretical studies.[41,42] The hydrodynamic interactions are screened, and the squeezed conformation behaves as a free-draining coil. Nevertheless, it should be reminded that due to intersegmental hydrodynamic interaction the intrinsic viscosity (not E_L/E_0, but E_L itself) is considerably reduced as compared to the free-draining limit, as shown in Table II.

It should be noted that eqs 33 and 34 used to model HI are based on some crude approximations. The basic equations underlying eqs 33 and 34 are those for the HI of a solid sphere with a single wall. Superimposing the single-wall contributions to model HI with two walls is a rather strong approximation.[35] Furthermore, the equations are based on a moving sphere in a quiescent solvent instead of a sphere in a Couette or Poiseuille flow giving rise to additional corrections not taken into account here.[35] Third, the HI of a chain with a wall is dealt with as the HI of a collection of $N + 1$ independently moving spheres; that is not a trivial assumption. Therefore, results on HI with the walls of a chain based on eqs 33 and 34 are likely to be only valid qualitatively. Especially at high shear rates, at small pores, and with a strong attractive interaction between chain segments and the walls, a more exact approach to model HI with the walls is desirable.

In Figure 6 the numerical calculated solutions of the Hookean dumbbell eqs 16 and 17 are plotted as a function of Δ. The parameter λ in terms of Δ is

$$\lambda = (3/4)(1/Q)\Delta^2 \qquad (47)$$

with $Q = 1.134$ (identifying R_0 with the end-to-end distance of the SAW) or $Q = 0.5562$ (identifying R_0 with twice the largest principal component of the radius of gyration).[14,38]

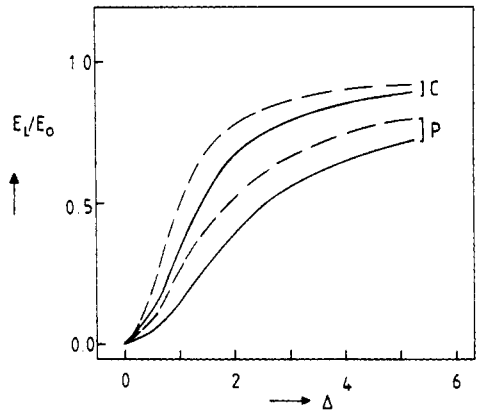

Figure 6. E_L/E_0 as a function of Δ, for a Hookean dumbbell:[31,32] (P) Poiseuille flow; (C) Couette flow. Solid lines: R_0 identified with the end-to-end distance of a SAW. Dashed lines: R_0 identified with twice the largest principal component of the radius of gyration of a SAW.

From Figure 6 and the limiting dumbbell eqs 18 and 19, it is clear that qualitatively the agreement between our own results and the dumbbell calculations is striking. In both models the intrinsic viscosity in Poiseuille flow is below its value in Couette flow. In both models for $\Delta \rightarrow \infty$ the values of intrinsic viscosities coincide. The differences between E_L/E_0 in Couette and Poiseuille flow are less than in our own model. Identification of R_0 with the end-to-end distance of the SAW gives the best fit to our results on Poiseuille flow. Identification of R_0 with twice the largest component of the radius of gyration gives the best fit to our results on Couette flow.

Concluding Remarks

The simulation model presented here on the zero-shear-rate intrinsic viscosity of a lattice chain allows easy incorporation of static and hydrodynamic interactions between segments and between segments and the walls. Results are in good agreement with free-draining calculations and with the dumbbell model of Goh et al.[31,32] In contrast to a dumbbell, the SAW chain is essentially flexible. The intrinsic viscosity in Poiseuille flow reaches its unbounded value at larger slit widths than in Couette flow. In Couette flow the intrinsic viscosity drops when the coils are squeezed, $\Delta \leq 1.5$.[7,14] The unbounded values of intrinsic viscosity in Couette and Poiseuille flow coincide.

It will be of interest to extend this work to cylindrical pores and porous media with random tortuous channels. The rather weak effect of the hydrodynamic interaction with the wall on the value of E_L/E_0 suggests that approximate expressions for the segment–surface hydrodynamic interactions will probably be sufficiently accurate for the purpose of treating the cylindrical and tortuous pore problem.

Although results presented here are for athermal SAW's (good solvent conditions), it is likely that these conclusions hold equally well for Θ solvents, as shown before explicitly for Couette flow, because the confinement will turn a Θ solvent into a "good" solvent.[7]

References and Notes

(1) Small, H. *J. Colloid Interface Sci.* **1974**, *48*, 147.
(2) Di Marzio, E. A.; Guttman, C. M. *Macromolecules* **1970**, *3*, 131.
(3) Chauveteau, G.; Tirrell, M.; Omari, A. *J. Colloid Interface Sci.* **1984**, *100*, 41.
(4) Zakin, J. L.; Hunston, D. L. *J. Macromol. Sci., Phys.* **1980**, *B18*, 795.
(5) Block, H. *Molecular Behavior and the Development of Polymeric Materials*; Ledwith, A., North, A. M., Eds.; Chapman & Hall: London, 1975.
(6) McCutchen, C. W. *Fed. Proc.* **1966**, *25*, 1061.
(7) van Vliet, J. H.; ten Brinke, G. *Macromolecules* **1991**, *24*, 5351.
(8) Omari, M.; Moan, M.; Chauveteau, G. *Rheol. Acta* **1989**, *28*, 520.
(9) Casassa, E. F. *Polym. Lett.* **1967**, *5*, 773.
(10) Casassa, E. F.; Tagami, Y. *Macromolecules* **1969**, *2*, 14.
(11) Davidson, M. G.; Suter, U. W.; Deen, W. M. *Macromolecules* **1987**, *20*, 1141.
(12) Casassa, E. F. *Macromolecules* **1984**, *17*, 601.
(13) Clark, A. T.; Lal, M. *J. Chem. Soc., Faraday. Trans. 2* **1981**, *77*, 981.
(14) van Vliet, J. H.; ten Brinke, G. *J. Chem. Phys.* **1990**, *93*, 1436.
(15) Churchill, S. W. *Viscous Flows: The Practical Use of Theory*; Butterworth: Boston, 1988.
(16) Bitsanis, I.; Magda, J. J.; Tirrell, M.; Davis, H. T. *J. Chem. Phys.* **1987**, *87*, 1733.
(17) Israelachvili, J. N.; Kott, S. J. *J. Colloid Interface Sci.* **1989**, *129*, 461.
(18) Gee, M. L.; McGuiggan, M.; Israelachvili, J. N.; Homola, A. M. *J. Chem. Phys.* **1990**, *93*, 1895.
(19) Hess, S.; Loose, W. *Phys. A.* **1989**, *162*, 138.
(20) Tirrell, M.; Malone, M. F. *J. Polym. Sci., Polym. Phys. Ed.* **1977**, *15*, 1569.
(21) Metzner, A. B.; Cohen, Y.; Rangel-Nafaile, C. *J. Non-Newtonian Fluid Mech.* **1979**, *5*, 449.
(22) Aubert, J. H.; Prager, S.; Tirrell, M. *J. Chem. Phys.* **1980**, *73*, 4103.
(23) Keh, K. J.; Anderson, J. L. *J. Chem. Phys.* **1984**, *80*, 1632.
(24) Wilkinson, M. K.; Gaunt, D. S.; Lipson, J. E. G.; Whittington, S. G. *Macromolecules* **1988**, *21*, 1818.
(25) Kramers, H. A. *J. Chem. Phys.* **1946**, *14*, 415.
(26) Zimm, B. H. *Macromolecules* **1980**, *13*, 592.
(27) Yamakawa, H. *Modern Theory of Polymer Solutions*; Harper & Row: New York, 1971.
(28) Rotne, J.; Prager, S. *J. Chem. Phys.* **1969**, *50*, 4831.
(29) Felderhof, B. U. *Phys. A* **1977**, *89*, 373.
(30) Debye, P. *J. Chem. Phys.* **1946**, *14*, 636.
(31) Goh, C. J.; Atkinson, J. D.; Phan-Thien, N. *J. Chem. Phys.* **1985**, *82*, 988.
(32) Goh, C. J.; Atkinson, J. D.; Phan-Thien, N. *J. Chem. Phys.* **1985**, *82*, 3442.
(33) Bird, B. R.; Curtiss, C. F.; Armstrong, R. C.; Hassager, O. *Dynamics of Polymer Solutions*, 2nd ed.; John Wiley & Sons: New York, 1987; Vol. 2.
(34) (a) Faxen, H. *Arkiv. Math. Astron. Fys.* **1923**, *17*, no. 27. (b) O'Neill, M. E. *Mathematika* **1964**, *11*, 67. (c) Goldman, A. J.; Cox, R. G.; Brenner, H. *Chem. Eng. Sci.* **1961**, *16*, 242. (d) Lorentz, A. H. *Abhandl. Theoret. Phys.* **1906**, *1*, 23. (e) Brenner, H.; Cox, R. G. *Chem. Eng. Sci.* **1967**, *22*, 1753. (f) Clark, A. T.; Lal, M.; Watson, G. M. *Faraday Discuss. Chem. Soc.* **1987**, *83*, 179.
(35) Happel, J.; Brenner, H. *Low Reynolds Number Hydrodynamics*, 2nd ed.; Martinus Nijhoff: Dordrecht, The Netherlands, 1973; Chapter 7.
(36) Flory, P. J. *Principles of Polymer Chemistry*; Cornell University Press: Ithaca, NY, 1972; Chapter XII.
(37) de Gennes, P.-G. *Scaling Concepts in Polymer Physics*; Cornell University Press: Ithaca, NY, 1979.
(38) Rapaport, D. C. *J. Phys. A: Math. Gen.* **1985**, *18*, 113.
(39) Madras, N.; Sokal, A. D. *J. Stat. Phys.* **1988**, *50*, 109.
(40) (a) Kuhn, W. *Kolloid-Z.* **1933**, *62*, 269; **1934**, *68*, 2. (b) Kuhn, W.; Kuhn, H. *Helv. Chim. Acta* **1943**, *26*, 194.
(41) Brochard, F. *J. Phys. (Les Ulis, Fr.)* **1977**, *38*, 1285.
(42) Brochard, F.; de Gennes, P.-G. *J. Chem. Phys.* **1977**, *67*, 52.